Open

LABORATORY SCIENCE

Influence of anterior capsulorhexis shape, centration, size, and location on intraocular lens position: finite element model

Tommaso Rossi, MD, Andrea Ceccacci, DEng, Gabriel Testa, PhD, Andrew Ruggiero, PhD, Nicola Bonora, PhD, Isabella D'Agostino, MD, Serena Telani, MD, Guido Ripandelli, MD

Purpose: To evaluate the influence of anterior capsulorhexis shape, dimension, and eccentricity on intraocular lens (IOL) position.

Setting: Laboratory investigation.

Design: Computational model.

Methods: A finite element model of the human crystalline lens capsule and zonule was created and the anterior capsule opened to simulate centered and decentered circular and elliptic rhexis. The model calculated capsular bag stress, IOL rotation, tilt, decentration, and vaulting, related to both capsular landmarks (absolute) and a reference IOL position defined as that obtained with a 5.0 mm circular and centered rhexis.

Results: Mean von Mises stress along the IOL major *z*-axis was significantly higher than that along the perpendicular *x*-axis in all cases ($P < .001$), both at the equator and at the rhexis edge. Stress at the equator was always greater than that at the rhexis edge ($P < .001$) regardless of the rhexis shape and position. As rhexis eccentricity increased, the stress difference between the *z*- and *x*-axes increased. Absolute IOL tilt (range 10^{-1} to 10^{-7} degrees), decentration (10^{-3} to 10^{-7} mm), rotation (10^{-2} to 10^{-3} degrees), and vaulting (10^{-1} mm) were negligible from an optical standpoint, but all of them were significantly greater for decentered rhexis (both round and elliptic) compared with centered ($P < .05$).

Conclusions: Anterior capsulorhexis irregularity and/or eccentricity increase IOL tilt, decentration, rotation, and vaulting in a numerically significant but optically negligible way. Von Mises stress is much greater at the capsular bag equator compared with the rhexis edge and highly asymmetrically distributed in all cases. Stress asymmetry may influence postoperative biologic processes of capsular bag shrinking and further IOL tilting or decentration.

J Cataract Refract Surg 2022; 48:222–229 Copyright © 2021 The Author(s). Published by Wolters Kluwer Health, Inc. on behalf of ASCRS and ESCRS

Cataract surgery is the most frequent surgical procedure of all medical fields with an estimated 3.6 million cases per year in the United States, 7 million in Europe, and 20 million worldwide. Phacoemulsification with intraocular lens (IOL) implant within the capsular bag is the state-of-the-art surgery achieving successful vision restoration in most patients.[1]

Proper IOL position within the capsular bag is a key factor in determining patients' postoperative refraction, and, therefore, quality of vision as anteroposterior displacement affects spherical equivalent, decentering causes aberration and a prismatic effect, rotation changes or vanishes cylinder correction, and tilting may result in astigmatism and/or iris chafing.[2]

The introduction of femtosecond laser–assisted cataract surgery (FLACS) allowed automation of some surgical maneuvers, including corneal incisions, anterior capsulorhexis, and lens fragmentation.[3] Among the presumed benefits of FLACS compared with manual surgery, the creation of a perfectly circular anterior capsulorhexis has been claimed to guarantee better IOL centering, whereas others affirm that no significant advantage can be demonstrated.[4,5]

Finite element modeling (FEM) has been extensively applied to ophthalmology in the past, and computational models of the eye, cornea, lens, mechanism of retinal trauma and accommodation created.[6,7] Although a certain variability of mechanical properties and the intrinsic anisotropy of biologic tissues impose caution in the interpretation of results and their transposition to the surgical theater, FEM is an invaluable tool for the analysis of forces applied to structures of known geometry and may offer important insight, especially when the clinical query is strictly related to force equilibrium, as in this case.

Submitted: March 1, 2021 | Final revision submitted: June 2, 2021 | Accepted: June 3, 2021

From the IRCCS Policlinico San Martino, Genoa, Italy (Rossi, D'Agostino, Telani), the Department of Civil and Mechanical Engineering DICeM, University of Cassino, Cassino, Italy (Testa, Ruggiero Bonora, Ceccacci); and IRCCS—Fondazione G.B. Bietti ONLUS, Rome, Italy (Ripandelli).

Corresponding author: Tommaso Rossi, MD, IRCCS Policlinico San Martino, L.go Rosanna Benzi 2, 16100 Genoa, Italy, Email: tommaso.rossi@usa.net.

0886-3350/$ - see frontmatter
https://doi.org/10.1097/j.jcrs.0000000000000711

The purpose of this article was to create a finite element model of the human capsular bag and Zinn zonule and to evaluate whether and find to what extent an eccentric and/or irregular rhexis shape influences IOL centering, rotation, and tilting within the capsular bag, inducing clinically significant optic aberrations.

METHODS

FEM Model

The profile geometry of the capsular bag was defined according to measures presented by Rosen et al.[8] Measurements ranged from 20 to 99 years, and equatorial diameter, anterior and posterior sagittal thickness, anterior and posterior curvature, and form factors were reported. Because data were age dependent and the authors defined analytical relation for all geometric factors, for the present study, as a reference, the age of 60 years was assumed. Thickness variation along the capsule profile was assumed according to Barraquer et al.[9]

Krag et al. tested a particular ring specimen extracted from the capsular bag to investigate the biomechanical characteristics of the human lens with respect to age and found that the capsular bag behavior is not linear.[10] To verify whether it was possible to assume a linear elastic material for the capsular bag, the ring test was simulated, considering the elastic modulus the Poisson ratio reported by Fisher for the reference age considered in this work.[11] As shown in Supplement Figure 1 (http://links.lww.com/JRS/A389), up to a strain of ~30%, the linear elastic material reproduces correctly the experimental measurements. For higher strain, the model can no more reproduce the tissue behavior, indicating that a different material model is necessary. However, because after IOL implantation, strain less than 30% was expected, the assumption of a linear elastic behavior can be justified.

To verify the accuracy of the material parameters, also the accommodation of the lens was simulated considering the capsule filled by the cortex and nucleus.[12] The cortex and nucleus were also assumed to be linear elastic materials.[13] As opposed to the IOL insertion, the geometry and loading conditions of this configuration were axisymmetric; then, a 2D model was implemented. Forces were used to model the zonular action. In particular, 3 different forces were applied with different vectors and acting on different areas.[14] This approach was consistent with that proposed by Hermans et al.[15] Variation of equatorial radius and lens thickness during accommodation were evaluated and compared with those measured by Lanchares et al.[16]

The IOL used to simulate the insertion was an EnVista MX60 from Bausch & Lomb. It is a single-piece foldable, aspheric biconvex lens made of hydrophobic acrylic material. IOL geometry is shown in Supplement Figure 2A (http://links.lww.com/JRS/A390) as a mesh used to discretize it. Esaedric elements were used because they are best suited for nonlinear conditions as the large displacements and contact expected in the simulation. Esaedric elements were also used for the capsular bag model, as shown in Supplement Figure 2B (http://links.lww.com/JRS/A391). The IOL was modeled as a linear elastic material.[17,18] The model used an elastic modulus of 4 MPa for the capsular bag (Poisson ratio 0.47) and 5.8 MPa for the hydrophobic acrylic IOL (Poisson ratio 0.39).

Stress and Main Outcome Measures

We separately modeled the capsular bag and IOL and then simulated IOL insertion within the capsular bag with the haptics fully folded against the optics, allowing the haptics to spread until reaching the equilibrium for all different anterior capsulorhexis shapes and positions schematically drawn in Supplement Figure 3 (http://links.lww.com/JRS/A391): (1) Circular rhexis centered on the geometric center of the capsular bag, with increasing diameters of 4.0 mm, 5.0 mm, 6.0 mm, and 7.0 mm; (2) Circular rhexis of 4.0 mm and 5.0 mm in diameter decentered along the *z*- and *x*-axes until tangent to the Zinn zonule insertion hypothesized at 7.0 mm[19]; (3) Elliptic rhexis of 6.0 mm by 4.0 mm centered on the geometric center of the capsular bag and oriented along the *z*- and *x*-axes; (4) Elliptic rhexis of 6.0 mm by 4.0 mm decentered along the *z*-axis and with the major axis oriented along the *z*- and *x*-axes, tangent to the Zinn zonule.

A perfectly circular anterior capsulorhexis of 5.0 mm in diameter, centered on the capsular bag *y*- (anteroposterior) axis, was considered the gold standard and the resulting IOL placement the reference artificial lens position. All displacements have been calculated as absolute values related to the capsular bag geometric center (Supplement Table 1, http://links.lww.com/JRS/A398) and as deltas compared with the reference IOL position (Table 1). The IOL was inserted within the capsular bag at surgical 6 to 12 hours and its major axis denominated *z* by convention, *x* its perpendicular on the IOL optic plate plane (surgical 3 to 9 hours), and *y* the axis perpendicular to the IOL plate plane (surgical anteroposterior axis).

IOL displacement was categorized under the following types for geometrical and optical reasons (Supplement Figure 4, http://links.lww.com/JRS/A392): (1) Rotation (around the *y*-axis) was defined as the angle between the IOL major axis at the time of insertion and after reaching the steady state; (2) Decentering was the distance between the projection of the geometric center of the IOL optic plate and the capsular bag *y*-axis; (3) Tilting (calculated on the *x*- and *z*-axes) was the angle comprised between the IOL optic plate and a plane perpendicular to the *y*-axis traced through the geometric center of the capsular bag; (4) Anteroposterior shifting (also referred to as vaulting) was defined as the IOL optic plate translation along the *y*-axis traced through the geometric center of the capsular bag.

Von Mises stress values at the equator and capsulorhexis margin were calculated for each rhexis configuration and displayed in cartesian axes where the rhexis edge and capsular bag equator angle position is reported in the abscissa and stress in the ordinate (Supplement Figures 5 through 9, http://links.lww.com/JRS/A393, http://links.lww.com/JRS/A394, http://links.lww.com/JRS/A395, http://links.lww.com/JRS/A396, and http://links.lww.com/JRS/A397).

The model calculated the effects of rhexis size, shape, and location on IOL decentration, tilting, rotation, and anteroposterior position, under each condition described.

Statistical Analysis

Statistical analysis used analysis of variance to evaluate the significance of von Mises stress values at different eccentricity along the rhexis edge and equator of the capsular bag of the different rhexis configurations. In all cases, *P* values of less than 0.05 were considered statistically significant.

RESULTS

Mean von Mises stress values along the *z*-axis (90 to 270 degree direction, same of the IOL major axis or surgical 6 to 12 hours) were significantly higher than those along the *x*-axis (0 to 180 degree direction) in all examined cases ($P < .001$ for all) regardless of the rhexis position and shape (Supplement Figures 5 through 9, http://links.lww.com/JRS/A393, http://links.lww.com/JRS/A394, http://links.lww.com/JRS/A395, http://links.lww.com/JRS/A396, and http://links.lww.com/JRS/A397), both at the capsular bag equator and at the rhexis edge. Also, stress at the capsular bag equator was always significantly greater than that at the rhexis edge ($P < .001$ in all cases) regardless of the rhexis shape and position (compare Supplement Figures 5A through 9A with Supplement Figures 5B through 9B, http://links.lww.com/JRS/A393, http://links.lww.com/JRS/A394,

Table 1. Results of Each Considered Rhexis Shape and Position Compared With the Reference IOL Position[a]

Configuration		Tilting (°)		A-P Shifting (mm)	Decentering (mm)		Rotation (°)
		Ax	αz	*y*	*x*	*z*	
Round centered	D = 4.0 mm	2.47E-05	−2.57E-06	−3.18E-02	2.32E-07	−1.20E-07	−4.00E-03
	D = 5.0 mm*	0*	0*	0*	0*	0*	0*
	D = 6.0 mm	1.02E-04	1.80E-05	−1.00E-03	2.06E-06	−1.00E-06	9.00E-03
	D = 7.0 mm	7.11E-05	1.80E-05	1.08E-01*	7.71E-07	−7.00E-09	1.70E-02*
	D = 8.0 mm	1.79E-05	9.36E-06	1.64E-01*	2.70E-07	2.20E-07	2.00E-02*
Round decentered D4.0 mm	(D4) *x* = 0; *z* = 1	3.70E-02	4.65E-03	−8.13E-02	3.11E-03	−4.53E-03	−2.40E-02
	(D4) *x* = 0; *z* = 2	1.03E-01*	9.18E-02	−5.09E-02	8.49E-03	−1.27E-02	−1.30E-02
	(D4) *x* = 1; *z* = 0	1.38E-01*	3.04E-02	−7.41E-02	1.67E-03	−1.24E-03	−1.80E-02
	(D4) *x* = 2; *z* = 0	1.58E-01*	5.62E-02	−7.73E-02	3.39E-03	−3.36E-03	−1.70E-02
Round decentered D5.0 mm	(D5) *x* = 0.5; *z* = 0	1.97E-01*	4.13E-02	−2.30E-02	1.66E-03	−1.41E-03	−5.00E-03
	(D5) *x* = 0; *z* = 0.5	2.57E-04	3.44E-02	−2.36E-02	1.52E-03	−2.39E-03	−1.20E-02
	(D5) *x* = 1; *z* = 0	1.25E-01*	3.14E-02	−1.82E-01*	2.44E-03	−1.97E-03	−5.60E-02
	(D5) *x* = 0; *z* = 1	7.18E-02*	5.52E-02	−3.52E-02	4.07E-03	−5.76E-03	−1.20E-02
Elliptic centered	6 by 4.0 mm *z*-axis	1.35E-03	5.75E-03	−7.30E-03	−1.40E-04	1.63E-04	−4.00E-03
	7 by 4.0 mm *z*-axis	1.61E-04	2.57E-05	1.60E-02	−1.70E-06	2.58E-06	−3.00E-03
	6 by 4.0 mm *x*-axis	3.66E-04	1.17E-04	−2.62E-02	−4.46E-06	3.19E-06	−4.00E-03
	7 by 4.0 mm *x*-axis	2.66E-04	3.80E-05	−2.73E-02	3.06E-06	−3.15E-06	−7.00E-03
Elliptic decentered	3 by 2.0 mm *z*-axis 0.5 mm Tangent to zonula	9.04E-03	5.58E-02	−1.68E-02	1.49E-03	−2.49E-03	−1.10E-02
	3 by 2.0 mm *x*-axis 0.5 mm	3.67E-01*	1.92E-01*	−2.53E-02	−4.94E-04	−7.15E-04	−2.00E-03

*Statistically significant difference compared with reference rhexis (5.0 mm wide and centered).
[a]Reference IOL position

http://links.lww.com/JRS/A395, http://links.lww.com/JRS/A396, and http://links.lww.com/JRS/A397).

Peak stress values at the capsular bag equator along the *z*-axis (90 to 270 degree angle position, where the haptics contact the capsule) were significantly greater than those along the perpendicular *x*-axis (0 to 180 degree angle position) for all considered rhexis shapes and positions ($P <$ .001 in all cases; Supplement Figures 5A through 9A, http://links.lww.com/JRS/A393, http://links.lww.com/JRS/A394, http://links.lww.com/JRS/A395, http://links.lww.com/JRS/A396, and http://links.lww.com/JRS/A397).

IOL position data for all rhexis diameter and shapes are reported in Supplement Table 1 (http://links.lww.com/JRS/A398) for absolute values related to capsular bag landmarks and compared with the reference position resulting from a 5 mm perfectly centered circular rhexis in Table 1. Absolute and relative rotations were within the range of 10^{-2} to 10^{-3} degrees in all cases.

Circular Rhexis (4.0 to 7.0 mm in Diameter) Centered on the Capsular Bag Axis

Tilting and decentering were negligible for all circular rhexis diameters. Vaulting decreased with an increase in the rhexis diameter and a maximum posterior dislocation of 0.47 mm for 4.0 mm rhexis (Supplement Table 1, http://links.lww.com/JRS/A398). Compared with the reference rhexis and IOL position, A-P shifting ranged between 10^{-1} and 10^{-3} mm (Table 1).

Peak stress values along the *z*-axis where the haptics contact the capsular bag (90 to 270 degree angle position) for 8.0 mm rhexis were significantly higher than other diameters ($P <$ .05) and along the *x*-axis (Supplement Figures 5A, http://links.lww.com/JRS/A393).

Stress at the rhexis edge (Supplement Figure 5B, http://links.lww.com/JRS/A393) was significantly lower ($P <$ .05) than that at the equator all-angle positions and followed a similar behavior. Stress values 180 degrees apart did not show a significant difference ($P \sim 1$ in all cases) regardless of the rhexis diameter, witnessing axial stress symmetry (Figure 1).

Circular Rhexis of 4.0 mm Diameter Decentered

Decentered rhexis of 4.0 mm diameter yielded IOL tilting of 10^{-1} degree at the most and decentering of 10^{-3} mm order of magnitude. Posterior vaulting was superior to centered rhexis values ($P <$ .05).

Von Mises stress at the capsular bag equator was significantly higher at the 270 degree angle position compared with 90 degrees ($P <$ .001) when decentering occurred along the *z*-axis, whereas for decentering along the *x*-axis, the difference was not significant (Figure 2).

Von Mises stress at the rhexis margin was significantly lower than bag equator and increased with higher degrees of decentering reaching the highest values at the 270 degree angle position for 2.0 mm decentering, being significantly higher than at 90 degrees ($P <$ .0001; Supplement Figure 6, http://links.lww.com/JRS/A394).

Circular Rhexis of 5.0 mm Diameter Decentered

Decentered rhexis of 5 mm diameter yielded IOL tilting of 10^{-1} degree at the most and decentering of 10^{-3} mm order

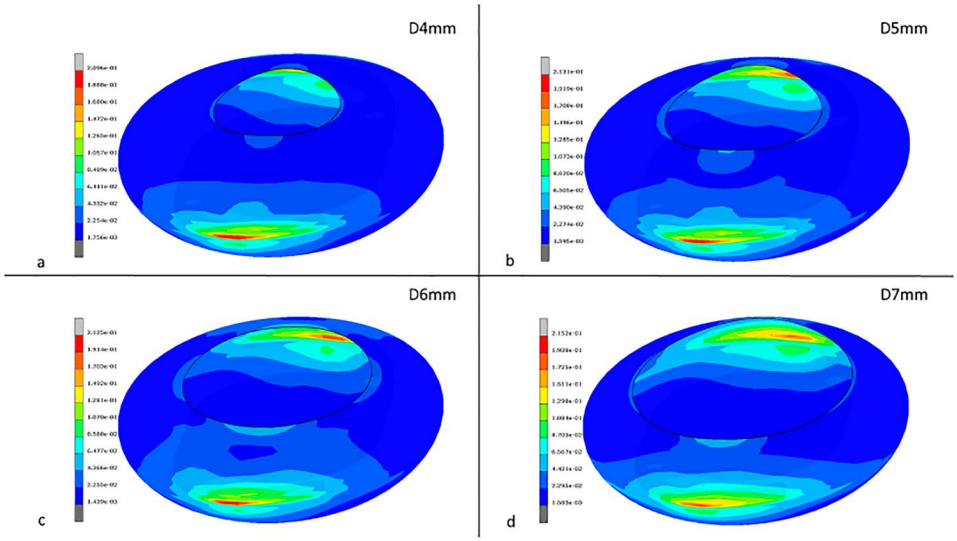

Figure 1. 3D drawing of capsular bag von Mises stress for a centered round rhexis of different diameters: (*A*) 4.0 mm, (*B*) 5.0 mm, (*C*) 6.0 mm, and (*D*) 7.0 mm.

of magnitude. Posterior vaulting was similar to centered rhexis values ($P > .05$).

Von Mises stress at the capsular bag equator was significantly higher than that at the rhexis margin at all positions ($P < .001$) and slightly but not significantly asymmetric, being higher at 270 degree angle position compared with 90 degrees ($P > .05$ for all cases; Supplement Figure 7, http://links.lww.com/JRS/A395).

Decentering along the *z*-axis (90 to 270 degrees) produced significantly higher stress than the corresponding rhexis diameter and the amount of decentering along the *x* (0 to 180 degrees) axis ($P < .001$ in all cases), and a higher degree of decentering along the same axis produced significantly more stress ($P < .001$; Figure 3).

Centered Elliptic Rhexis

Tilting ranged in the 10^{-3} to 10^{-5} degrees and decentering between 10^{-7} and 10^{-4} mm, whereas anteroposterior shifting ranged between 10^{-1} and 10^{-3} mm compared with the reference IOL position.

Mean IOL tilting along the *z*- and *x*-axes of all decentered rhexis (any diameter, both circular and elliptic) was significantly greater than that of centered rhexis ($P < .01$); mean IOL decentering also was higher for decentered rhexis compared with centered ones ($P < .05$). Anteroposterior shifting and rotation did not show a significant difference among centered and decentered rhexis.

Peak stress values along the *z*-axis where the haptics contact the capsular bag (90 to 270 degree angle position) were significantly higher for the 4 by 2.0 mm ellipsis compared with all others (Figure 4; $P < .05$). Capsular bag stress along the *z*-axis was significantly higher than that along the *x*-axis for all considered ellipses ($P < .001$ for all comparisons). Stress at the rhexis edge was significantly lower for all ellipses shaped and orientations except for the 4 by 2.0 mm along the *z*-axis ($P < .05$) compared with the stress at the capsular bag equator.

Rhexis edge stress at 90 to 270 degree angle positions showed significant variation at 90 to 270 degree angle positions ($P < .001$ in all cases) among ellipses with the

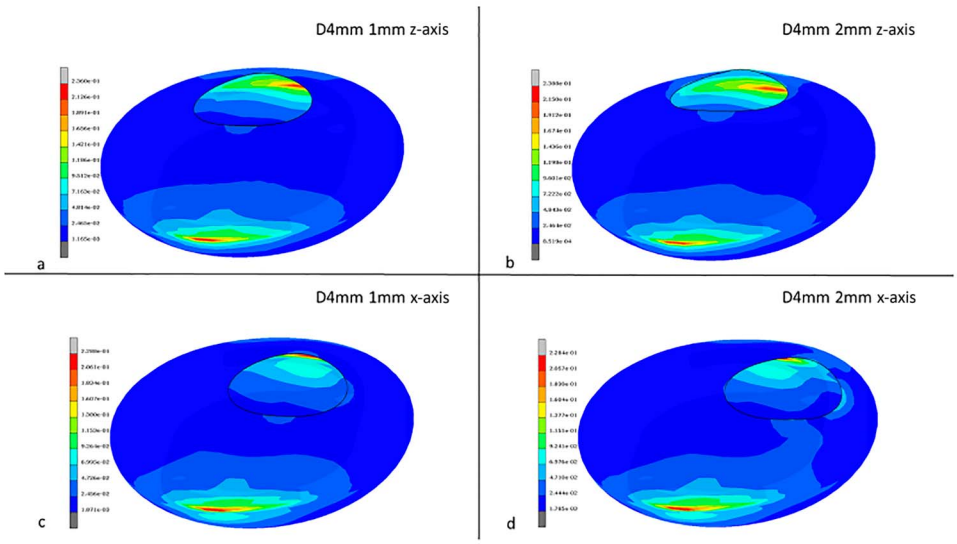

Figure 2. 3D drawing of capsular bag von Mises stress for decentered 4 mm round rhexis: (*A*) 1 mm decentration along the *z*-axis; (*B*) 2.0 mm along the *z*-axis; (*C*) 1.0 mm along the *x*-axis; and (*D*) 2.0 mm along the *x*-axis.

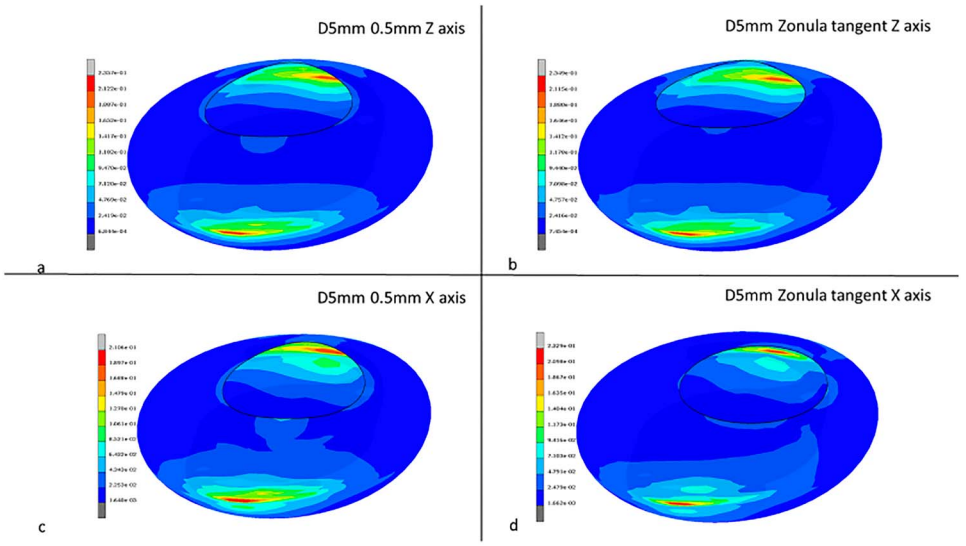

Figure 3. 3D drawing of capsular bag von Mises stress for decentered 5 mm round rhexis: (*A*) 0.5 mm decentration along the *z*-axis; (*B*) tangent to the zonule along the *z*-axis; (*C*) 0.5 mm along the *x*-axis; and (*D*) tangent to the zonule along the *x*-axis.

major axis along the *z*-axis, whereas elliptic rhexis with their major axis along the *x*-axis showed a significant stress increase at the rhexis edge at 0 to 180 degrees as the major axis increased (Supplement Figure 8, http://links.lww.com/JRS/A396). Stress values 180 degrees apart did not show a significant difference ($P \sim 1$ in all cases) regardless of the rhexis diameter, witnessing axial stress symmetry.

Decentered Elliptic Rhexis

Tilting ranged in the 10^{-1} to 10^{-3} degrees and decentering between 10^{-7} mm and 10^{-4} mm, whereas anteroposterior shifting ranged within 10^{-2} mm compared with the reference IOL position.

Peak stress values along the *z*-axis where the haptics contact the capsular bag (90 to 270 degree angle position) were not significantly different between the 2 studied cases (Figure 5). Capsular bag stress at the equator was slightly but not significantly asymmetric, being higher at 270 degrees compared with 90 degrees for the ellipsis with a major axis along the *x*-axis.

Stress at the rhexis edge was significantly lower for both decentered cases (Supplement Figure 9, http://links.lww.com/JRS/A397; $P < .05$) compared with the stress at the capsular bag equator and markedly asymmetric for the ellipsis parallel to the *x*-axis, showing stress at 270 degrees significantly greater than that at 90 degrees ($P < .001$).

DISCUSSION

Effective IOL position after cataract surgery greatly affects refraction, particularly if toric and multifocal lenses are implanted. Manual continuous circular capsulorhexis (CCC) represents the state-of-the-art technique for capsular bag content removal and IOL insertion, offering consistent rim stability and stress resistance.[20]

Femtosecond laser–assisted cataract surgery creates anterior capsulorhexis through contiguous laser bursts in a postage stamp perforation fashion, yielding a circular and centered capsulotomy. This may cause less IOL tilt and decentration compared with CCC but reduces the capsule tensile strength because of laser-induced microfractures

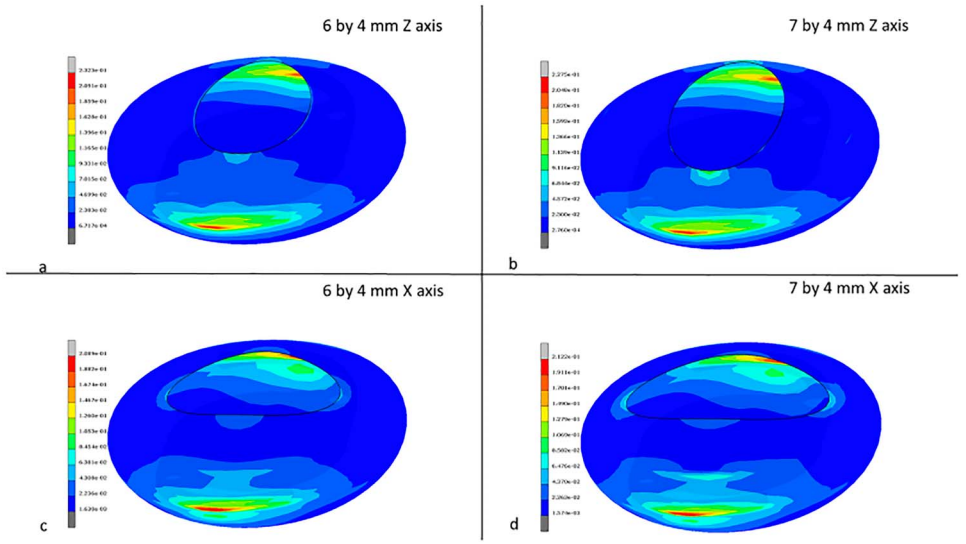

Figure 4. 3D drawing of capsular bag von Mises stress for centered elliptic rhexis: (*A*) 6 by 4.0 mm along the *z*-axis; (*B*) 7 by 4.0 mm along the *z*-axis; (*C*) 6 by 4.0 mm along the *x*-axis; and (*D*) 7 by 4.0 mm along the *x*-axis.

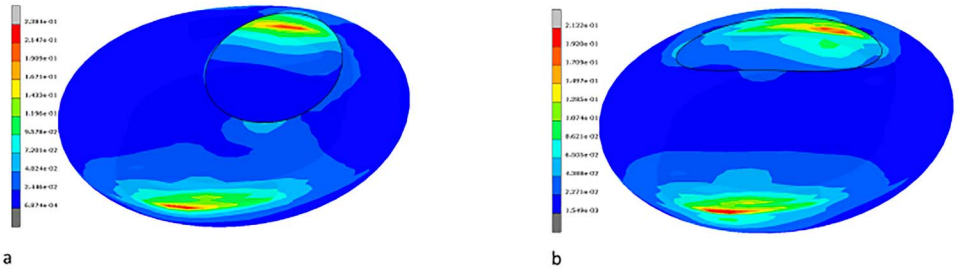

Figure 5. 3D drawing of capsular bag von Mises stress for decentered elliptic rhexis: (*A*) 6 by 4.0 mm along the *z*-axis tangent to the zonule and (*B*) 6 by 4.0 mm along the *x*-axis tangent to the zonule.

and increases the risk for capsular tear, tags, and incomplete capsulotomy.[4,21,22]

Our study considers all degrees of freedom for IOL position because they all affect refraction and quality of vision through optical aberrations: tilt induces astigmatism, decentration creates prismatic effects and aberration, anteroposterior shifting changes the spherical equivalent, and rotation alters toric corrections.

Stress, IOL tilt, and decentration significantly changed as a function of rhexis shape and position (Supplement Table 1, http://links.lww.com/JRS/A398 and Table 1): those differences, although numerically relevant, appear optically negligible. Tilt and decentration do increase with rhexis irregularity and decentration but remain extremely modest: between 10^{-1} to 10^{-7} degrees and 10^{-2} to 10^{-7} mm, respectively, both related to capsular landmarks and reference IOL. It should be noted that the crystalline lens position shows a significant interpersonal variation with mean inferotemporal tilting of 4 degrees and 0.1 mm decentering to the temporal side, values close to Findl data referred to over 250 patients 3 months after cataract extraction with CCC, which would seem to have left them substantially unaltered.[23,24] Gu et al. also found a correlation between IOL and crystalline lens tilt and axial length in a cohort of patients operated on with CCC.[25]

The posterior IOL shifting of 0.44 mm (Supplement Table 1, http://links.lww.com/JRS/A398) that we calculated for reference position (the one obtained with a round and centered rhexis of 5.0 mm) is expected with this particular IOL design because of the angled haptics intended to displace the optic plate away from the posterior iris surface. Of interest, any further displacement from this reference position and attributable to rhexis enlargement and/or decentration is negligible (10^{-1} to 10^{-3} mm range; Table 1).

Rotation data related to capsular bag landmarks (all within 10^{-2} degree range; Supplement Table 1, http://links.lww.com/JRS/A398) are clinically insignificant in all tested cases but may retain surgical value for the development of a newer haptic design as they help predict toric IOL final position after reaching the equilibrium between haptics deployment and capsular bag elasticity. Lai et al. found no significant difference in toric IOL rotation and the final visual outcome when comparing a manual CCC vs FLACS.[26]

Cornaggia et al. investigated the effect of the size and position of the rhexis on the IOL decentering and tilt with FEM making simplifying assumptions.[27] In their work, the IOL was simulated as a prescribed force applied to the capsule, the extension of the contact area is assumed arbitrarily, neglecting that during the haptics extension the contact area changes, the force distribution varies and the capsular bag stretch, as it was already considered flattened. The authors found that increasing the rhexis size and decentering also increases tilting. Assuming prescribed force instead to simulate the interaction between the IOL and the capsular bag, tilting was evaluated considering the entire capsule rotation and displacement. It becomes difficult to compare the results, as in the present study, tilting and decentering were directly measured on the IOL because the capsular bag was considered sustained by the Zinn zonule that cannot allow the capsule to tilt.

IOL position within the capsular bag is the resulting at equilibrium between the elastic force applied by IOL haptics against the capsular bag equator and the resistance offered by it, which, in turn, depends on its mechanical properties, shape, and the elastic force exerted by the Zinn zonule. Because the elastic modulus of hydrophobic acrylic IOLs (such as the one we modeled) is higher than that of hydrophilic acrylic ones, the former was used as reference material to cause higher stress in the lens capsule, thus investigating a more critical condition.

The design of IOLs intended for capsular bag placement varies considerably in terms of haptics shape, number, and angulation. All geometries are intended to exercise symmetric elastic force against the capsular bag walls enabling self-placement of the haptics against the capsular bag equator and self-centering of the optic plate.

Stress distribution across the lens capsule (Figures 1 to 5) changes significantly with rhexis shape and position: mean stress at the capsular bag equator is always greater than that at the corresponding rhexis margin except for round 4.0 mm rhexis decentered by 2.0 mm along the *z*-axis (Figures 2, *A* and *B*). Even more importantly, stress along the *z*-axis (90 to 270 degree direction) where the haptics contact the bag at the capsular bag equator is much greater than that across the orthogonal axis (Figures 1, *A* through 5, *A*) for all considered cases ($P <$ .001 all cases), whereas at the rhexis margin, stress is much lower (Figures 1, *B* through 5, *B*). Li et al. found a correlation between asymmetric rhexis diameters and IOL stability that relates to asymmetric stress, in agreement with our model.[28] They also reported that

plate optic IOL designs tend to associate with less horizontal rhexis diameter change over time, possibly because of better stress distribution along the capsular bag equator, as a consequence of a greater arc of contact compared with J-loop shapes.

Our model shows that this behavior as stress at the rhexis margin greatly increases when the rhexis is decentered (Figures 2, *B*, 3, *B*, 5, *B*), especially if this occurs along the *z*-axis where the haptics exert their elastic force. It should be noted that rhexis diameters after IOL implant depend both on the original shape and on stretching forces exerted by the haptics: IOL shapes yielding wider contact onto the capsular bag equator distribute stress more evenly and may be less prone to decentration over time, thanks to a lesser disproportion between orthogonal rhexis axis tension. Of interest, Lee et al. demonstrated that the use of a capsular tension ring reduced long-term IOL tilting and decentering after uneventful cataract surgery, suggesting that 360 degree stress distribution around the capsule equator increases IOL stability.[29]

Although our model necessarily referred to a single-IOL design, most implanted IOLs have similar shapes with limited capsular contact along the major axis, mostly to facilitate injection. It is therefore reasonable to expect that they all concentrate stress along a single axis. Different IOL geometry resulting in larger haptics–capsule contact such as the plate-haptics, double C-loop, and four closed haptics distributes forces on a larger surface, generating lower stress.

Biologic processes ensuing with time impact IOL position: the anterior chamber depth increases immediately after surgery and reduces in the subsequent days per week; the capsular bag shrinks up to 0.5 mm and becomes more oval.[30,31] After YAG laser capsulotomy, such forces relax and the capsular bag significantly changes its shape once again, altering IOL tilt and decentration thereafter.[32]

In summary, our model shows numerically significant changes in IOL position due to rhexis centering and shape, although the clinical and refractive relevance seems negligible given the exceedingly small calculated values: Ashena et al. demonstrated that decentration less than 0.2 mm and tilting up to 4 degrees have very limited impact in aberrometry and vision quality even when toric or multifocal IOLs were considered.[33]

It is important to highlight that finite elements compute forces resulting from the surgical procedure producing a specific rhexis shape and clarify their mechanical significance. From that very moment on, biology enters the game and possibly takes the lead: collagen protein shrinkage and cell proliferation start remodeling the entire zonule–capsular bag–IOL system, although mechanics keeps playing a prominent role. Stress retains well-known effects on gene expression documented also within the eye, and it is conceivable that collagen modifications exacerbate, with time, any imbalance generated by force asymmetry.[34] In other words, the uneven distribution of stress along the capsular bag equator may influence gene expression resulting in long-term asymmetric fibrosis and consequent shape modifications impacting lens position in the long run.

The quest for perfect rhexis remains open, as CCC gives better stability and rhexis strength, whereas FLACS results in virtual shape perfection, although both techniques end up producing overlapping visual results. Our study suggests that future research should also focus on IOLs made of materials and designed in shapes that distribute stress more evenly across the equator and the entire capsular bag as this is another major player in long-term lens stability and refractive reliability.

Acknowledgments

The authors thank Fondazione Roma for support.

WHAT WAS KNOWN

- Anterior capsulorhexis irregularity influences force vectors across the entire capsular bag
- Femtolaser rhexis can be more centered and regular than manual continuous circular capsulorhexis
- The effective clinical and refractive relevance of such difference in rhexis precision between manual and laser rhexis is still a matter of debate

WHAT THIS PAPER ADDS

- The numerical value of tilting, decentering, and rotation induced by even macroscopic capsulorhexis irregularity is mathematically relevant but optically negligible
- Stress along the capsular bag equator is much greater than that at the rhexis margin

REFERENCES

1. Ianchulev T, Litoff D, Ellinger D, Stiverson K, Packer M. Office-based cataract surgery: population health outcomes study of more than 21 000 cases in the United States. Ophthalmology 2016;123:723–728
2. Ortiz C, Esteve-Taboada JJ, Belda-Salmerón L, Monsálvez-Romín D, Domínguez-Vicent A. Effect of decentration on the optical quality of two intraocular lenses. Optom Vis Sci 2016;93:1552–1559
3. Nagy ZZ, Mastropasqua L, Knorz MC. The use of femtosecond lasers in cataract surgery: review of the published results with the LenSx system. J Refract Surg 2014;30:730–740
4. Kránitz K, Miháltz K, Sándor GL, Takacs A, Knorz MC, Nagy ZZ. Intraocular lens tilt and decentration measured by Scheimpflug camera following manual or femtosecond laser-created continuous circular capsulotomy. J Refract Surg 2012;28:259–263
5. Sachers F, Goldblum D. Kapsulorhexis Real-Life—erfahrener Operateur versus Literaturdaten zur Femto Laser Assisted Cataract Surgery (FLACS) [Capsulorhexis Real-Life—experienced Surgeon versus Femto Laser Assisted Cataract Surgery (FLACS) as Reported in Literature]. Klin Monbl Augenheilkd 2018;235:409–412
6. Rossi T, Boccassini B, Esposito L, Clemente C, Iossa M, Placentino L, Bonora N. Primary blast injury to the eye and orbit: finite element modeling. Invest Ophthalmol Vis Sci 2012;53:8057–8066
7. Rossi T, Boccassini B, Esposito L, Iossa M, Ruggiero A, Tamburrelli C, Bonora N. The pathogenesis of retinal damage in blunt eye trauma: finite element modeling. Invest Ophthalmol Vis Sci 2011;52:3994–4002
8. Rosen AM, Denham DB, Fernandez V, Borja D, Ho A, Manns F, Parel JM, Augusteyn RC. In vitro dimensions and curvatures of human lenses. Vis Res. 2006;46:1002–1009
9. Barraquer RI, Michael R, Abreu R, Lamarca J, Tresserra F. Human lens capsule thickness as a function of age and location along the sagittal lens perimeter. Invest Ophthalmol Vis Sci 2006;47:2053–2060
10. Krag S, Olsen T, Andreassen TT. Biomechanical characteristics of the human anterior lens capsule in relation to age. Invest Ophthalmol Vis Sci 1997;38:357–363

11. Fisher RF. Elastic constants of the human lens capsule. J Physiol 1969;201: 1–19
12. Pedrigi RM, David G, Dziezyc J, Humphrey JD. Regional mechanical properties and stress analysis of the human anterior lens capsule. Vis Res. 2007;47:1781–1789
13. Wang K, Venetsanos D, Wang J, Pierscionek BK. Gradient moduli lens models: how material properties and application of forces can affect deformation and distributions of stress. Sci Rep 2016;6:31171
14. Michael R, Mikielewicz M, Gordillo C, Montenegro GA, Pinilla Cortés L, Barraquer RI. Elastic properties of human lens zonules as a function of age in presbyopes. Invest Ophthalmol Vis Sci 2012;53:6109–6114
15. Hermans EA, Dubbelman M, van der Heijde GL, Heethaar RM. Estimating the external force acting on the human eye lens during accommodation by finite element modelling. Vis Res 2006;46:3642–3650
16. Lanchares E, Navarro R, Calvo B. Hyperelastic modelling of the crystalline lens: accommodation and presbyopia. J Optom 2012;5:110–120
17. Bozukova D, Werner L, Mamalis N, Gobin L, Pagnoulle C, Floyd A, Liu E, Stallings S, Morris C. Double-C loop platform in combination with hydrophobic and hydrophilic acrylic intraocular lens materials. J Cataract Refract Surg 2015;41:1490–1502
18. Tehrani M, Dick HB, Wolters B, Pakula T, Wolf E. Material properties of various intraocular lenses in an experimental study. Ophthalmologica. 2004; 218:57–63
19. Lim SJ, Kang SJ, Kim HB, Kurata Y, Sakabe I, Apple DJ. Analysis of zonular-free zone and lens size in relation to axial length of eye with age. J Cataract Refract Surg 1998;24:390–396
20. Reyes Lua M, Oertle P, Camenzind L, Goz A, Meyer CH, Konieczka K, Loparic M, Halfter W, Henrich PH. Superior rim stability of the lens capsule following manual over femtosecond laser capsulotomy. Invest Ophthalmol Vis Sci 2016;57:2839–2849
21. Avetisov KS, Bakhchieva NA, Avetisov SE, Novikov IA, Belikov NV, Khaydukova IV. Biomechanical properties of the anterior lens capsule after manual and femtolaser capsulotomy [in English, Russian]. Vestn Oftalmol 2019;135:4–11
22. Wang J, Su F, Wang Y, Chen Y, Chen Q, Li F. Intra and post-operative complications observed with femtosecond laser-assisted cataract surgery versus conventional phacoemulsification surgery: a systematic review and meta-analysis. BMC Ophthalmol 2019;19:177
23. Hirnschall N, Buehren T, Bajramovic F, Trost M, Teuber T, Findl O. Prediction of postoperative intraocular lens tilt using swept-source optical coherence tomography. J Cataract Refract Surg 2017;43:732–736
24. Findl O, Hirnschall N, Draschl P, Wiesinger J. Effect of manual capsulorhexis size and position on intraocular lens tilt, centration, and axial position. J Cataract Refract Surg 2017;43:902–908
25. Gu X, Chen X, Yang G, Wang W, Xiao W, Jin G, Wang L, Dai Y, Ruan X, Liu Z, Luo L, Liu Y. Determinants of intraocular lens tilt and decentration after cataract surgery. Ann Transl Med 2020;8:921
26. Lai KR, Zhang XB, Yu YH, Yao K. Comparative clinical outcomes of Tecnis toric IOL implantation in femtosecond laser-assisted cataract surgery and conventional phacoemulsification surgery. Int J Ophthalmol 2020;13:49–53
27. Cornaggia A, Clerici LM, Felizietti M, Rossi T, Pandolfi A. A numerical model of capsulorhexis to assess the relevance of size and position of the rhexis on the IOL decentering and tilt. J Mech Behav Biomed Mater 2021;114:104170
28. Li S, Hu Y, Guo R, Shao Y, Zhao J, Zhang J, Wang J. The effects of different shapes of capsulorrhexis on postoperative refractive outcomes and the effective position of the intraocular lens in cataract surgery. BMC Ophthalmol 2019;19:59
29. Lee DH, Shin SC, Joo CK. Effect of a capsular tension ring on intraocular lens decentration and tilting after cataract surgery. J Cataract Refract Surg 2002;28:843–846
30. Sato T, Shibata S, Yoshida M, Hayashi K. Short-term dynamics after single- and three-piece acrylic intraocular lens implantation: a swept-source anterior segment optical coherence tomography study. Sci Rep 2018;8: 10230
31. de Castro A, Rosales P, Marcos S. Tilt and decentration of intraocular lenses in vivo from Purkinje and Scheimpflug imaging. Validation study. J Cataract Refract Surg 2007;33:418–429
32. Uzel MM, Ozates S, Koc M, Taslipinar Uzel AG, Yılmazbaş P. Decentration and tilt of intraocular lens after posterior capsulotomy. Semin Ophthalmol 2018;33:766–771
33. Ashena Z, Maqsood S, Ahmed SN, Nanavaty MA. Effect of intraocular lens tilt and decentration on visual acuity, dysphotopsia and wavefront aberrations. Vision (Basel) 2020;4:41
34. Kirwan RP, Fenerty CH, Crean J, Wordinger RJ, Clark AF, O'Brien CJ. Influence of cyclical mechanical strain on extracellular matrix gene expression in human lamina cribrosa cells in vitro. Mol Vis 2005;11:798–810

Disclosures: *None reported.*

First author:
Tommaso Rossi, MD

IRCCS Policlinico San Martino, Genoa, Italy